Metallophysics and Advanced Technologies
Металофіз. новітні технол.
Metallofiz. Noveishie Tekhnol.
2026, vol. 48, No. 8, pp. 775–789
https://doi.org/10.15407/mfint.48.08.0775
Reprints available directly from the publisher

© 2026 G. V. Kurdyumov Institute for Metal Physics,
National Academy of Sciences of Ukraine
Published by license under
the G. V. Kurdyumov Institute for Metal Physics–
N.A.S. of Ukraine Publishers imprint.
Printed in Ukraine.

PACS numbers: 61.43.Gt, 61.72.sh, 64.75.Lm, 81.05.Rm, 81.20.Ev, 88.30.R-

Influence of LaH_x Additions on Characteristics of TiFe-Based Hydrogen-Storage Alloys Manufactured *via* Hydrogen-Assisted Powder Metallurgy

Z. Liu[*,**], Y. Wang[*,**], T. Cheng[*,**], Y. Song[*,**], D. Savvakin[*,**,***], N. Li[****], and O. Ivasishin[*,**,***]

[*]*College of Materials Science and Engineering,*
Jilin University,
CN-130012 Changchun, China
[**]*International Center of Future Science,*
Jilin University,
CN-130012 Changchun, China
[***]*G. V. Kurdyumov Institute for Metal Physics, N.A.S. of Ukraine,*
36 Academician Vernadsky Blvd.,
UA-03142 Kyiv, Ukraine
[****]*State Key Laboratory of Materials Processing and Die & Mould Technology,*
Huazhong University of Science and Technology,
CN-430074 Wuhan, China

TiFe-based alloys are promising candidates for solid-state hydrogen storage due to their low cost and excellent reversibility near room temperature. However, the conventional powder metallurgy (PM) manufacturing method often induces severe surface oxidation of Ti powders, which significantly hinders the activation and degrades the hydrogen-storage capacity of produced TiFe alloys. In this work, low-cost TiFe-based alloys are synthesized *via* hydrogen-assisted powder-metallurgy route. To mitigate the oxygen impurity issue, La hydride (LaH_x) is introduced as an oxygen scavenger and pore-forming agent. The results indicate that the addition of La plays a dual role: it reacts with

Corresponding author: Orest Mykhaylovych Ivasishin
E-mail: orest.ivasyshyn@gmail.com

Citation: Z. Liu, Y. Wang, T. Cheng, Y. Song, D. Savvakin, N. Li, and O. Ivasishin, Influence of LaH_x Additions on Characteristics of TiFe-Based Hydrogen-Storage Alloys Manufactured *via* Hydrogen-Assisted Powder Metallurgy, *Metallofiz. Noveishie Tekhnol.*, **48**, No. 8: 775–789 (2026). DOI: 10.15407/mfint.48.08.0775

© Publisher PH 'Akademperiodyka' of the NAS of Ukraine, 2026. This is an open access article under the CC BY-ND license (https://creativecommons.org/licenses/by-nd/4.0)

oxygen to form stable La oxides, thereby reducing the oxygen content within the main TiFe matrix, and creates a porous microstructure that facilitates hydrogen redistribution inside the material. Characterization by O/N/H analysis and XRD confirms that, while the total oxygen content increases with La doping, the formation of La-oxide precipitations reduces the concentration of oxygen dissolved in the TiFe matrix. Consequently, the La-doped alloy exhibits superior activation properties and a reversible hydrogen-storage capacity of 0.96% wt. at 40°C compared to 0.58% wt. for the undoped alloy. This study provides a feasible strategy for preparing high-performance TiFe-based alloys *via* a cost-effective PM route.

Key words: TiFe alloy, La hydride, hydrogen-assisted powder metallurgy, pore-forming effect, hydrogen-storage capacity.

Стопи на основі сполуки TiFe є перспективними матеріялами для твердофазного зберігання Гідроґену завдяки їхній низькій вартості та здатності оборотньо взаємодіяти з Гідроґеном за кімнатної температури. Проте, стандартні порошкові технології виготовлення цих стопів часто призводять до надмірного окиснення поверхні порошків, що перешкоджає активації стопу та понижує здатність накопичувати Гідроґен. У цій роботі стопи на основі TiFe було синтезовано методою порошкової металурґії з використанням наводнених порошків. Щоб зменшити проблему з домішкою Оксиґену, гідрид La (LaH_x) був введений як вбирач Оксиґену та пороутворювач. Результати показують, що додавання La відіграє подвійну роль: він реаґує з Оксиґеном, утворюючи стабільні оксиди La, тим самим зменшуючи вміст Оксиґену в основній матриці TiFe, та створює пористу мікроструктуру, яка сприяє перерозподілу Гідроґену всередині матеріялу. Дослідження спеченого стопу за допомогою аналізи O, N, H і рентґенівської дифракції підтверджує, що, хоча загальний вміст Оксиґену збільшується з La-леґуванням, утворення виділень оксиду La зменшує концентрацію Оксиґену, розчиненого в матриці TiFe. Леґований La стоп демонструє чудові активаційні властивості й оборотню водневу місткість (0,96% мас.) за 40°C порівняно з 0,58% мас. для нелеґованого стопу. Це дослідження пропонує можливу стратегію одержання високоефективних стопів на основі TiFe за допомогою економічно ефективного порошкового підходу.

Ключові слова: стоп TiFe, гідрид Лантану, воднева порошкова металурґія, ефект пороутворення, воднева місткість.

(Received 8 July, 2026; in final version, 16 July, 2026)

1. INTRODUCTION

The escalating global energy crisis has propelled the hydrogen industry into the spotlight, driven by hydrogen high energy-density and clean-combustion characteristics [1–8]. Within this sector, hydrogen storage and transportation are pivotal. Conventional methods, such as high-pressure gaseous and cryogenic-liquid storage, are hampered by significant drawbacks, including safety risks and high energy con-

sumption, respectively [3, 6]. Solid-state hydrogen storage emerges as a promising alternative, offering high volumetric capacity and enhanced safety [8–10]. Among various solid-state materials, TiFe-based alloys are particularly attractive due to their low cost and excellent reversibility near ambient temperatures [11, 12].

The synthesis of TiFe alloy is commonly achieved through arc melting, mechanical alloying, and powder metallurgy [13–19]. Arc melting produces an as-cast microstructure with coarse grains, which lengthens the diffusion path of hydrogen and limits the hydrogen-storage kinetic properties of the alloy [15]. Mechanical alloying tends to cause cold welding of powder particles, which requires the addition of organic process-control agents and introduces carbon impurities consequently [16]. In contrast, powder metallurgy, specifically hydrogen-assisted powder sintering, presents distinct advantages, including a simple process and low production cost [18, 20, 21]. The inherent porosity in sintered alloys provides effective pathways for hydrogen diffusion, optimizing kinetic behaviour [19, 22].

However, the powder-metallurgy route faces a critical challenge—the severe surface oxidation of Ti powders during processing. This oxide layer acts as a barrier, hindering hydrogen diffusion, impeding activation, and degrading the overall hydrogen-storage capacity [23]. Previous studies have confirmed that a high oxygen concentration suppresses the formation of the primary TiFe phase and that dissolved oxygen in the TiFe matrix can destabilize the metal hydride by reducing the desorption enthalpy [24]. Therefore, precise control of oxygen content is paramount for enhancing the alloy performance.

To mitigate the detrimental effects of surface oxidation, recent studies have explored the use of La-based additives. Chen *et al.* demonstrated that adding LaH_3 to V–Ti–Cr–Fe alloys decreased the proportion of titanium oxides and improved hydrogen adsorption–desorption capacity [25]. Similarly, Alam *et al.* found that, in mechanically alloyed TiFe, the *in situ* formation of LaH_3 promoted heterogeneous pores' nucleation and provided diffusion channels for hydrogenation [26]. These findings suggest that rare-earth doping is an effective strategy for oxygen control, where the additive reduces the oxygen content in alloy matrix, weakens surface oxide layers, and accelerates hydrogen diffusion *via* the formation of LaH_3.

In this work, we fabricate both pure and La-doped TiFe alloys, using a cost-effective hydrogen-assisted powder-metallurgy route. We introduce La hydride (LaH_x) as a dual-function additive serving as both an oxygen scavenger and a pore-forming agent. A series of characterization tests are conducted to investigate systematically the synergistic regulatory effect of La doping on the microstructure and hydrogen-storage performance. This study aims to clarify the intrinsic modification mechanism of La, focusing on its role in powder activation, phase

formation, and the optimization of hydrogen adsorption/desorption thermodynamics and kinetics. Our findings reveal a cooperative mechanism, wherein La doping constructs hydrogen-diffusion channels, while achieving purification of TiFe lattice, providing practical guidance for optimizing the fabrication of high-performance TiFe-based hydrogen-storage materials.

2. MATERIALS AND METHODS

2.1. Preparation of TiFe Alloys

TiH_2 powder (99.9% purity, < 45 μm) and pure iron powder (99.9% purity, < 38 μm) were adopted as raw materials. The atomic ratio of Ti and Fe was fixed at 1:1 for all samples. 1% wt. La hydride (< 38 μm) was introduced into one group, while the other group contained no additive. The two groups of weighed powders were placed into a container and mixed in a powder-mixing machine at 30 rpm for 6 hours. The as-obtained Ti–Fe mixed powders were loaded into a mould, sealed under vacuum, and then subjected to cold isostatic pressing at 300 MPa with a holding time of 300 s. The green compacts were placed in a vacuum sintering furnace. Upon reaching a vacuum level of $1{\cdot}10^{-3}$ Pa, the furnace was heated at a rate of 10°C/min. After completion of the dehydrogenation stage, the temperature was maintained at 1200°C for 2 hours, followed by furnace cooling to room temperature.

2.2. Characterization

Phase identification was conducted by x-ray diffraction (XRD, PANalytical Empyrean) using CuK_α radiation from 20° to 90° at a scan rate of 10°/min. Oxygen content was measured by an O/N/H analyser (LECO-ONH 836). The microstructure and elemental distribution were observed by scanning electron microscopy (SEM, Thermo Fisher Verios 5 UC) equipped with energy-dispersive x-ray spectroscopy (EDS). Room-temperature compression tests were carried out on a universal testing machine (MTS-E43.104) at a strain rate of 1 mm/min, with specimen dimensions of ∅5 mm×10 mm.

2.3. Hydrogen-Storage Performance Measurement

All samples were activated and tested under equal experimental conditions. To activate hydrogen sorption, vacuum heat treatment was performed at 700°C to reduce the thickness of the surface oxide film. The initial hydrogenation conducted at 700°C under 50 bar hydrogen pressure was adopted to expose the fresh alloy matrix. Ten adsorption–

desorption cycles were subsequently carried out to stabilize the hydrogen-storage capacity. Finally, pressure–composition–temperature (PCT) tests were performed at 40°C on a hydrogen adsorption–desorption instrument (H-Sorb X600PCT-Pro, CIQTEK) to evaluate the hydrogen-storage performance.

3. RESULTS AND DISCUSSION

3.1. Pore-Forming Effect of La Addition

Figure 1 shows the metallographic micrographs of undoped and La-doped TiFe alloys, illustrating the differences in micromorphology and pore structure between the two samples. Low-magnification images show that interconnected macropores exist in both specimens, while the La-doped alloy contains a substantially larger amount of macropores. High-magnification metallographic observations further exhibit the matrix microstructure [27]. Micropores can be found in the undoped sample, yet the La-doped TiFe matrix contains much denser and more abundant micropores. The comparison demonstrates that La-doping promotes the development of both macropores and micropores and produces a well-developed dual-scale porous structure.

Figure 2 shows the SEM morphologies and elemental distribution

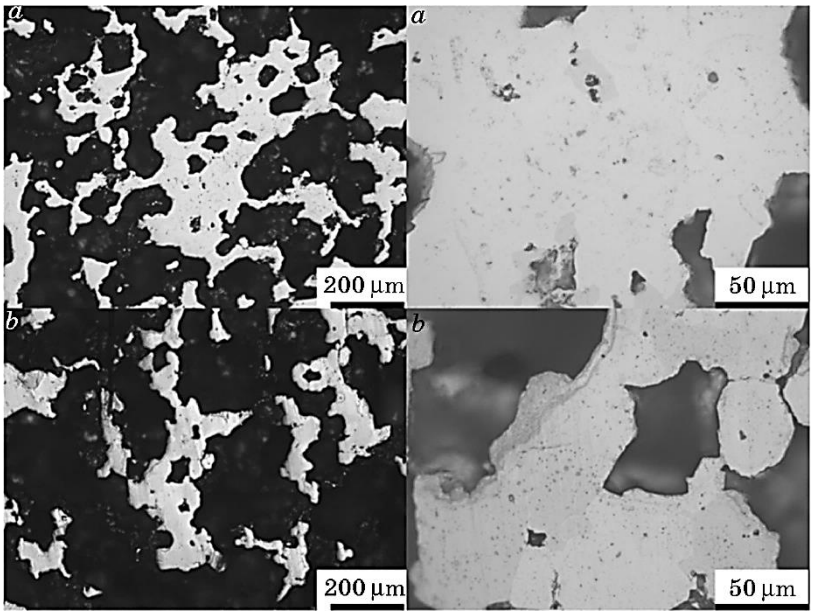


Fig. 1. Metallographic images of undoped and La-doped TiFe alloys at different magnifications: undoped alloy (*a*), La-doped alloy (*b*).

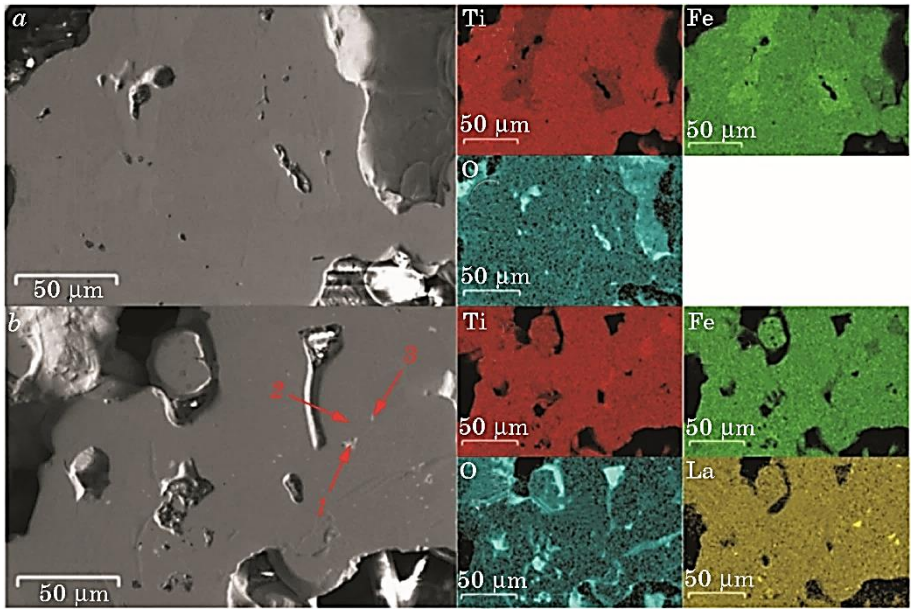


Fig. 2. SEM morphologies and elemental distribution mappings of undoped and La-doped TiFe alloys: undoped alloy (*a*), La-doped alloy (*b*). The marked points in Fig. 2, *b* represent the selected regions for EDS point scanning.

mappings of undoped and La-doped TiFe alloys. Ti and Fe elements exhibit inhomogeneous distribution in both samples. The signal intensity of Ti and Fe declines obviously within the pore areas, indicating low concentrations of Ti and Fe on pore walls and interiors. In contrast, oxygen displays obvious localized enrichment in many pore regions, including large pores and tiny micropores. In the La-doped sample, prominent La signals emerge mainly in partial micropore areas, where oxygen is also enriched. Comparatively, strong La signals are barely observed on large pores that indicates that La-containing phases tend to aggregate preferentially within the micropores rather than large pores.

To further explore the elemental composition difference between micropore regions and dense matrix regions of the La-doped sample, three positions marked in Fig. 2, *b* were selected for EDS point scanning. The atomic percentages of Ti, Fe, O and La at these testing points are summarized in Table 1. Point 1 and point 3 are in micropore regions. The results show extremely low Ti and Fe contents, while O and La account for the overwhelming majority, with combined atomic percentages exceeding 90%. In contrast, point 2 is situated in the dense matrix area away from micropores. This position is dominated by Ti and Fe, and only a small amount of oxygen can be detected; nearly, no

TABLE 1. Elemental composition gained by EDS point scanning at the marked spots in Fig. 2, *b*.

Points	Ti, % at.	Fe, % at.	O, % at.	La, % at.
1	2.1	1.5	61.9	34.5
2	48.2	44.9	6.8	0.0
3	4.2	2.4	60.5	32.9

La element exists in this region. The quantitative data further verify that La and O tend to accumulate within the micropores of the La-doped TiFe alloy forming small precipitations (particles of 2 μm in size).

Combined with metallographic observation, SEM morphology, and EDS elemental analysis results, the effect of La-doping on the microstructure of TiFe alloy can be clarified. The undoped TiFe alloy contains inherent pores after sintering. After La-doping, the macropore size of the alloy increases obviously, while the number of internal micropores rises significantly. SEM and EDS tests confirm that La and O elements preferentially accumulate in micropore regions rather than in dense matrix areas. The enrichment of La and O inside the micropores induces the generation of abundant micropores. In general, La-doping effectively promotes the formation and development of the dual-scale pore structure of sintered TiFe alloy.

3.2. Effect of La Addition on Oxygen Redistribution in the Material

The phase composition of undoped and La-doped TiFe alloys was characterized by XRD, and the corresponding patterns are presented in Fig. 3. Both samples contain the main TiFe phase together with the impurity Ti_4Fe_2O phase [27]. Ti_4Fe_2O forms during high-temperature sintering *via* reactions between the alloy matrix and trace residual oxygen. This impurity phase exerts a poisoning effect on the hydrogen-storage system of TiFe-based alloys [28]. Clear differences in phase constituents are identified between the two samples. Compared with the undoped TiFe alloy, new diffraction peaks belonging to La_2O_3 emerge in the XRD pattern of the La-doped specimen [29]. The appearance of the La_2O_3 phase verifies that the doped La element possesses strong oxygen affinity and consumes partial oxygen impurities in the alloy matrix during the sintering process. Since partial oxygen participates in the formation of La_2O_3, the oxygen source for generating the harmful Ti_4Fe_2O phase is reduced correspondingly [30]. This competitive oxygen-consumption behaviour inhibits the generation of detrimental Ti_4Fe_2O phase with La-doping.

O/N/H analysis was further adopted to characterize quantitatively

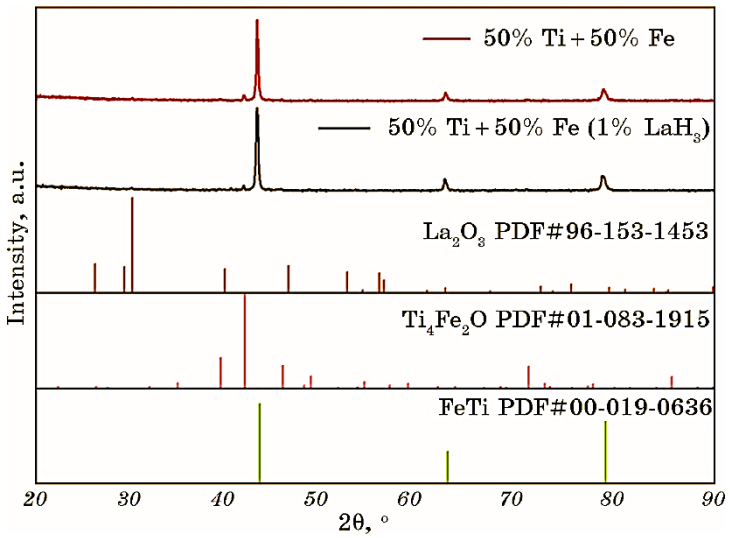


Fig. 3. X-ray diffraction patterns of undoped and La-doped alloys.

TABLE 2. Oxygen, nitrogen and hydrogen contents of undoped and La-doped alloys.

Samples	O, % wt.	N, % wt.	H, % wt.
undoped alloy	0.306	0.00577	0.00426
La-doped alloy	0.472	0.00581	0.0109

the variation of oxygen content, and the measured data are summarized in Table 2. The total oxygen content does not decrease after La-doping, but it shows obvious upward trend. This observation suggests that noticeable part of oxygen impurity can be introduced in the alloy with initial lanthanum hydride powder. What is more important, the effect of La-doping leads to a redistribution of oxygen inside the sintered alloy material. This leads to purification (deoxidization) of the TiFe lattice (matrix) rather than of the sintered material as a whole. This trend can be explained with the support of previous SEM observations and EDS mapping as well as point scanning results.

Multiple characterization results demonstrate jointly that La is not uniformly distributed in the sintered TiFe alloy, but accumulates as small precipitations preferentially within the micropores and grain-boundary regions. Owing to high oxygen affinity, La drives oxygen impurities to migrate out from the TiFe-alloy matrix toward porous and defective zones. The migrated oxygen reacts preferentially with enriched La to generate La_2O_3 precipitations rather than forming Ti_4Fe_2O inside the matrix [31].

Consequently, although La addition increases the statistical total oxygen content of the alloy in macroscopic measurement, the formation of La_2O_3-phase precipitations fundamentally enables the effective deoxidation of the alloy matrix, reducing the oxygen impurity dissolved in the TiFe crystal lattice. The oxygen impurities, which originally poisoned the hydrogen-storage performance, are transferred and consumed in the defect regions that reduces the content of harmful Ti_4Fe_2O phase in the matrix and purifies the alloy microstructure. Furthermore, the *in situ* generation of La_2O_3 particles in pore regions is consistent with the pore-forming effect concluded in the previous section. The oxygen migration and phase-transformation behaviour induced by La-doping achieve simultaneously matrix purification and microstructure optimization, which provides an improved matrix structure for the hydrogen-storage reaction of TiFe alloy.

3.3. Compressive Mechanical Performance

Room-temperature compression tests were carried out to investigate the mechanical performance of undoped and La-doped TiFe alloy. Figure 4 presents the compressive stress–strain curves of the two samples. Table 3 summarizes the corresponding average peak compressive stress and fracture strain. The stress–strain curves show obvious differences between the two alloys. The undoped TiFe alloy achieves a higher peak stress, while the La-doped TiFe alloy exhibits a delayed

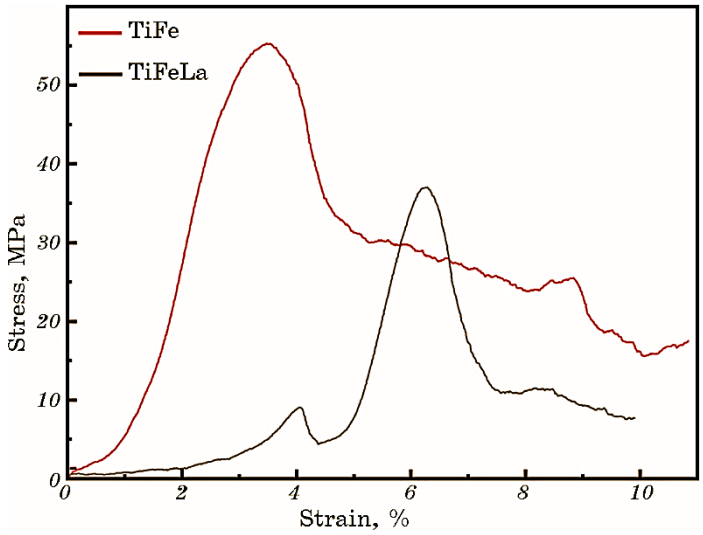


Fig. 4. Representative compressive stress–strain curve of undoped and La-doped TiFe alloys.

TABLE 3. Average peak compressive stress and fracture strain of undoped and La-doped TiFe alloys. Data are expressed as mean ± standard deviation.

Sample	Stress, MPa	Strain, %
undoped alloy	60.1 ± 6.79	8.04 ± 3.96
La-doped alloy	32.25 ± 6.72	11.47 ± 2.23

peak position. Combined with the statistical data in Table 3, the average peak compressive stress of undoped TiFe alloy is of (60.10 ± 6.79) MPa, which reduces to (32.25 ± 6.72) MPa for La-doped TiFe alloy. In terms of fracture strain, undoped TiFe alloy reaches $(8.04 \pm 3.96)\%$, whereas La-doped TiFe alloy increases to $(11.47 \pm 2.23)\%$.

The variation of mechanical properties can be associated with the microstructure evolution induced by La-doping. As discussed above, La addition promotes the *in situ* formation of La_2O_3 particles and generates abundant micropores within the alloy matrix. Under compressive load, these micropores and dispersed La_2O_3 particles act as stress-concentration sites, accelerating crack initiation and propagation and lowering the bearing capacity of the alloy. Meanwhile, the porous microstructure provides space for plastic deformation, which accounts for the larger fracture strain of La-doped TiFe alloy.

These results demonstrate that La-doping reduces the peak compressive strength and improves the deformability of undoped TiFe alloy. From the perspective of practical processing, the decline in compressive strength brings favourable advantages for the hydrogen-storage TiFe alloys. La-doped TiFe alloy can be crushed into fine particles under lower external force, simplifying subsequent pulverization and granulation procedures [32]. Combined with foregoing discussion, La-doping inducing La_2O_3 formation simultaneously realizes TiFe-matrix deoxidation and pore construction, regulating alloy mechanical properties. Such comprehensive modification improves the machinability of TiFe-based alloys and facilitates subsequent activation and hydrogen-storage applications [30].

3.4. PCT Hydrogen-Storage Performance

Figure 5 presents the PCT curves for the undoped and La-doped TiFe alloys at 40°C. The PCT measurements reveal significant differences in both the plateau characteristics and the hydrogen-adsorption capacity between the two samples. The undoped TiFe sample exhibited a sloping-plateau region spanning approximately 10–25 bar (1–2.5 MPa). The hydrogen concentration increased substantially as the pressure was raised. At the end of this plateau region, the hydrogen-adsorption capacity reached approximately 0.58% wt. Upon further pressuriza-

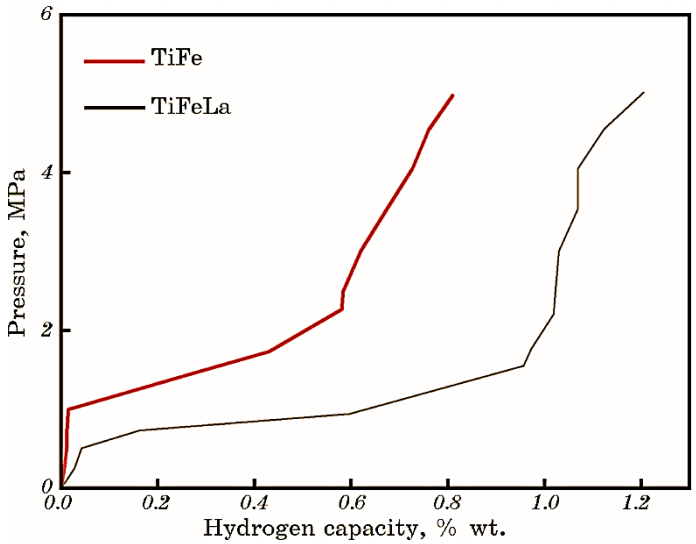


Fig. 5. PCT curves for the undoped and La-doped TiFe alloys at 40°C.

tion to 50 bars, the hydrogen concentration continued to rise gradually, ultimately reaching 0.81% wt. In striking contrast, the La-doped TiFe sample displayed a considerably flatter plateau, with the majority of hydrogen adsorption occurring within the narrow pressure window of 5–15 bars. Within this short interval, the hydrogen concentration increased rapidly to approximately 0.96% wt., exceeding the plateau-end capacity of the undoped sample. Upon further pressurization to 50 bar (5 MPa), the total hydrogen concentration reached approximately 1.20% wt., which is 0.39% wt. higher than the value obtained for the undoped sample.

The markedly improved hydrogen-storage performance of the La-doped sample can be rationalized on the basis of prior XRD, SEM–EDS and O/N/H analyses. The XRD and O/N/H analyses have demonstrated that La-doping reduces the amount of Ti_4Fe_2O phase through preferential oxygen scavenging, preserving the chemical purity of the TiFe matrix [33]. Since Ti_4Fe_2O is an inert phase that does not participate in hydrogen adsorption, its removal is directly contributing to the higher total capacity. Simultaneously, the pore-forming effect of La (increase in total volume of dual-scale pore structure) provides a more extensive network of hydrogen-transport pathways. The enhanced porosity facilitates the infiltration of hydrogen gas into the interior of the sample, accelerating the kinetics of hydrogen uptake and enabling a more complete utilization of the TiFe matrix. The steeper plateau observed in the La-doped sample (5–15 bars *vs.* 10–25 bar) suggests that the improved pore network reduces the pressure hysteresis in sintered TiFe

alloys.

The synergy between the pore-forming and matrix purification of La-doping is therefore evident in the PCT behaviour: the deoxidation effect increases the intrinsic hydrogen-storage capacity of the matrix by reducing the inactive Ti_4Fe_2O phase, while the pore-forming effect enhances the hydrogen accessibility and uptakes kinetics through the creation of a more open microstructural network [19]. This dual mechanism—chemical purification of TiFe matrix coupled with physical channel creation—accounts for the simultaneous increase in both the plateau capacity (0.96% wt. *vs.* 0.58% wt.) and the ultimate capacity (1.20% wt. *vs.* 0.81% wt.) of the La-doped sample.

3.5. Phase Constitution and Impurity Variations after PCT Cycling

To investigate the phase stability and internal elemental variation of undoped alloy and La-doped alloy after long-term hydrogen adsorption and desorption cycling, XRD phase characterization and O/N/H analysis were performed on the cycled alloy samples. The phase structural changes before and after cycling were analysed, based on the XRD results, while the variations of oxygen and hydrogen elements were summarized and discussed, according to the O/N/H test data.

XRD test results shown in Fig. 6 reveal that no new diffraction peaks are observed for the undoped alloy after PCT cycling. In comparison, a new diffraction signal appears for the La-doped alloy, which can

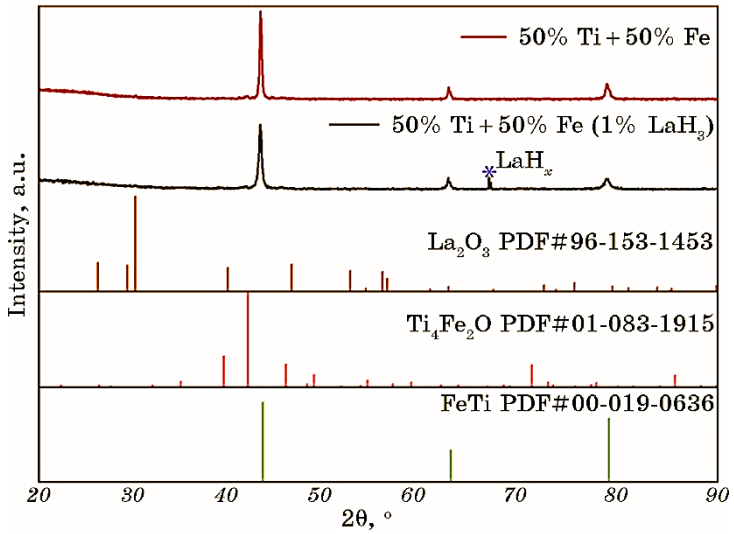


Fig. 6. XRD patterns for the undoped alloy and La-doped alloy after PCT hydrogen absorption–desorption cycling.

TABLE 4. O/N/H elemental contents of alloys before and after PCT cycling.

Samples	O, % wt.	N, % wt.	H, % wt.
undoped alloy	0.760	0.0293	0.0295
La-doped alloy	0.749	0.0357	0.0897

be preliminarily assigned to La-hydride phase (marked in Fig. 6). This indicates that the La-containing phases in the matrix, such as La oxide, can react with hydrogen upon PCT cycling to form La hydride.

As summarized in Table 4, residual hydrogen content rises for both alloys after PCT cycling, while a considerably higher magnitude increase is observed for the La-doped alloy. Accordingly, it may be inferred that La-containing phases (*e.g.*, La oxide) within the La-doped alloy react with hydrogen to produce La hydride. This inference is well supported by the foregoing XRD observations.

Combining the above XRD and O/N/H characterization results, the two sets of experimental evidence jointly indicate that La-bearing constituents inside the La-doped alloy undergo hydrogenation reactions during PCT cycling to produce La hydride.

4. SUMMARY

In this work, we studied comparatively microstructure, mechanical properties and hydrogen-storage performance of TiFe alloy and La-doped TiFe alloy fabricated by hydrogen-assisted powder sintering. The addition of La brought an evident pore-forming effect inside the matrix, modifying the internal pore structure of sintered samples. Moreover, La-doping realized local accumulation of oxygen impurity with formation of lanthanum-oxide precipitations in TiFe matrix, removing harmful Ti_4Fe_2O phase and purifying the TiFe lattice.

Compression-test results demonstrated that the La-doped alloy possessed lower compressive strength relative to the undoped alloy. This reduced strength facilitates crushing the alloy into fine powder particles, which supports subsequent activation and practical application for hydrogen storage.

PCT characterization confirmed the improvement in hydrogen-storage performance derived from La modification. The La-doped alloy exhibited a smoother and more stable hydrogen-adsorption platform. Its hydrogen-storage capacity on the platform was higher than that of the undoped alloy, and the ultimate hydrogen capacity measured at 5 MPa outperformed the undoped counterpart too.

Characterizations after hydrogen adsorption–desorption cycling show increased residual hydrogen content in both alloys. A higher hydrogen increment can be observed for the La-doped alloy. It can be con-

cluded that La hydride is formed through the reaction between La-bearing phases and hydrogen during cycling.

In summary, La-doping optimizes the microscopic structure, crushability and overall hydrogen-storage performance of the TiFe alloys.

This work was financially supported by the National Natural Science Foundation of China (Nos. 52441402 and 52301047), Scientific Research Project of Education Department of Jilin Province (JJKH20261265KJ) and Jilin Province Science and Technology Development Plan Item (20260205066GH). The authors also gratefully acknowledge financial support from Jilin University, China and the National Academy of Sciences of Ukraine.

AUTHORS' CONTRIBUTIONS

Zheyu Liu: experimentation, analysis, drafting; Yuanmeng Wang: analysis, drafting; Yuchao Song: conception and design, provision of resources, supervision, reviewing, and editing; Dmytro Savvakin: data organization, reviewing; Ning Li: data organization, editing; Orest Ivasishin: reviewing, validation.

REFERENCES

1. Z. Li, B. Guan, K. Shu, L. Zhu, T. Zhu, Z. Zhuang, X. Hu, C. Zhu, S. Zhao, J. Chen, J. Gao, H. Dang, L. Zhang, Y. Li, L. Xu, W. Zeng, S. Chen, L. Wang, C. Zhu, J. He, Q. Xian, and Z. Huang, *Int. J. Hydrogen Energy*, **204**: 153160 (2026).
2. S. Kurbanbekov, M. Skakov, V. Tskhe, Y. Amangeldiyeva, A. Gradoboev, A. Tokezhanov, D. Baltabayeva, and N. Raimzhanova, *Metals*, **16**, Iss. 7: 720 (2026).
3. W. Fang, C. Ding, L. Chen, W. Zhou, J. Wang, K. Huang, R. Zhu, J. Wu, B. Liu, Q. Fang, X. Wang, and J. Wang, *Energy and Fuels*, **38**, Iss. 15: 13539 (2024).
4. M. R. Kalibek, A. D. Ospanova, B. Suleimenova, R. Soltan, T. Orazbek, A. M. Makhmet, K. S. Rafikova, and N. Nuraje, *Discover Nano*, **19**: 195 (2024).
5. T. H. Le, M. P. Kim, C. H. Park, and Q. N. Tran, *Materials*, **17**, Iss. 3: 666 (2024).
6. P. K. Panigrahi, B. Chandu, M. R. Motapothula, and N. Puvvada, *Energy and Fuels*, **38**, Iss. 4: 2630 (2024).
7. R. Etezadi, S. Shivaramakrishnan, R. Wang, R. Khalighi, L. Zhao, I. G. Eschrich, F. Aquino, M. Ibrahim, C. Tasser, and T. T. Tsotsis, *Industrial Eng. Chem. Research*, **65**, Iss. 3: 1403 (2026).
8. R. Murugavel, A. A. Rownaghi, P. A. Webley, and F. Rezaei, *Energy and Fuels*, **39**, Iss. 38: 18251 (2025).
9. M. G. Nijkamp, J. E. M. J. Raaymakers, A. J. van Dillen, and K. P. de Jong, *Appl. Phys. A*, **72**: 619 (2001).
10. B. Weinberger and F. D. Lamari, *Int. J. Hydrogen Energy*, **34**: 3058 (2009).

11. H. Liu, J. Zhang, P. Sun, C. Zhou, Y. Liu, and Z. Z. Fang, *J. Energy Storage*, **68**: 107772 (2023).
12. Y. Xu, Y. Deng, W. Liu, X. Zhao, J. Xu, and Z. Yuan, *Sustainable Energy Technologies and Assessments*, **55**: 102974 (2023).
13. E. I. L. Gymez, K. Edalati, F. J. Antiqueira, D. D. Coimbrro, G. Zepon, D. R. Leiva, T. T. Ishikawa, J. M. Cubero-Sesin, and W. J. Botta, *Advanced Eng. Mater.*, **22**, Iss. 10: 2000011 (2020).
14. K. Oishi, S. Takagi, Y. Daikuhara, T. Haraki, H. Uchida, M. Abe, T. Kokaji, and S. Uchida, *J. Advanced Sci.*, **16**, No. 2: 46 (2004).
15. A. Knaislová, P. Novák, J. Kopeček, and F. Průša, *Materials*, **12**, Iss. 19: 3084 (2019).
16. R. B. Falcão, E. D. C. C. Dammann, C. J. da Rocha, and R. M. L. Neto, *Mater. Sci. Forum*, **600–661**: 329 (2010).
17. J. Umeda, T. Tanaka, T. Teramae, S. Kariya, J. Fujita, H. Nishikawa, Y. Shibutani, J. Shen, and K. Kondoh, *Mater. Sci. Eng. A*, **803**: 140708 (2021).
18. A. O. Araoyinbo, F. A. Ishola, E. Y. Salawu, M. B. Biodun, and A. U. Samuel, *AIP Conf. Proc.*, **2437**: 020153 (2022).
19. H. Zhang, Y. Liu, G. Miao, Z. Ma, F. Sun, A. Ju, X. Qu, and P. Li, *Chem. Eng. J.*, **526**: 171450 (2025).
20. J. M. Torralba, *Metals*, **11**, Iss. 10: 1519 (2021).
21. L. Radmann, A. C. Domingos Dias Moraes, L. V. Biehl, R. M. Lima, B. P. d. Silva, M. C. d. Souza, and J. L. B. Medeiros, *Sustainability*, **18**, Iss. 10: 5065 (2026).
22. W. J. Yan, Y. B. Tao, and H. Ye, *Int. J. Hydrogen Energy*, **86**: 1154 (2024).
23. H. Shi, Y. Zhang, Z. Li, F. Gao, X. Wang, Y. Yang, Y. Liu, X. Xiao, F. Fang, and W.-G. Cui, *Int. J. Minerals, Metallurgy Mater.*, **32**: 2743 (2025).
24. H. Liu, J. Zhang, P. Sun, C. Zhou, Y. Liu, and Z. Z. Fang, *J. Energy Storage*, **55**: 105543 (2022).
25. Z. Chen, L. Luo, Z. Su, W. Liu, F. Zhang, and Y. Huang, *Int. J. Hydrogen Energy*, **44**: 13538 (2019).
26. M. M. Alam, P. Sharma, and J. Huot, *Int. J. Hydrogen Energy*, **50**: 261 (2024).
27. Q. Zhao, Z. He, Y. He, Y. Qiu, Z. Wang, and J. Yao, *Intermetallics*, **162**: 108004 (2023).
28. K. Hiebl, E. Tuscher, and H. Bittner, *Chemischer Informationsdienst*, **10**, Iss. 19: 38 (1979).
29. M. M. Alam, P. Sharma, and J. Huot, *Int. J. Hydrogen Energy*, **50**: 727 (2024).
30. X. Wei, W. Chen, X. He, L. Wang, D. Jiao, and Y.-Q. Fu, *Int. J. Hydrogen Energy*, **208**: 153293 (2026).
31. Z. Hou, S. Guo, X. Zhang, L. Xu, Y. Qi, Y. Zhang, P. Li, and D. Zhao, *Int. J. Hydrogen Energy*, **136**: 469 (2025).
32. Y. Xu, Y. Zhou, Y. Li, Y. Hao, P. Wu, and Z. Ding, *Molecules*, **29**, Iss. 11: 2451 (2024).
33. Z. Han, X. Gao, J. Li, Z. Huang, X. Kang, T. Zhai, H. Sun, Z. Yuan, L. Wang, and X. He, *Int. J. Hydrogen Energy*, **239**: 155454 (2026).